Multi-mode lasing in terahertz metasurface quantum-cascade VECSELs

Yu Wu,[1, a)] Sadhvikas Addamane,[2] John L. Reno,[2] and Benjamin S. Williams[1]

[1]*Department of Electrical and Computer Engineering, University of California, Los Angeles, California 90095, USA*

[2]*Sandia National Laboratories, Center of Integrated Nanotechnologies, MS 1303, Albuquerque, New Mexico 87185, USA*

[a)] Electronic mail: ywu17@ucla.edu

Abstract:

Up to now, terahertz quantum-cascade vertical-external-cavity surface-emitting lasers (QC-VECSELs) have tended to oscillate in only one or two lasing modes at a time. This is due to the fact that the interaction between all of the longitudinal external cavity modes and the QC gain material is mediated through a single metasurface resonance whose spatial overlap changes little with frequency; this suppresses spatial-hole-burning induced multi-mode operation. In this Letter, a VECSEL external cavity is demonstrated using an output coupler based upon a high-resistivity silicon etalon which presents a periodic reflectance spectrum that is nearly matched with the external cavity mode spectrum. As the cavity length is varied, a systematic transition between a single/double-mode lasing regime and a multi-mode lasing regime is realized due to Vernier effect. Up to nine modes lasing simultaneously with a free-spectral-range of approximately 21 GHz is demonstrated. This result provides a path towards the multi-mode operation necessary for eventual frequency comb operation.

The manuscript

The demand for high-resolution, broadband, and fast spectroscopy/sensing in THz frequency range has promoted the study of THz quantum-cascade (QC) laser based frequency combs.[1–5] The QC material itself exhibits a broadband spectral response and octave-spanning multi-mode lasing has been demonstrated in waveguide-based THz QC-lasers, typically with mode spacings in the range of 5-20 GHz as set by the free-spectral-range (FSR).[6] Such dense multi-mode

operation is a prerequisite for realizing fully coherent frequency combs. Many physical mechanisms can drive a laser from a single-mode regime to a multi-mode regime, e.g. spatial and spectral hole burning, saturable absorption, and population pulsations.[7–9] In waveguide-based THz QC-lasers, spatial hole burning (SHB) is believed to be particularly important, since the non-uniform longitudinal standing wave modal intensity creates spatially non-uniform gain saturation. The resulting population grating has a period of tens of microns, which is too large to be smoothed out by diffusion given the picosecond gain recovery times in QC-lasers.

THz quantum-cascade vertical-external-cavity surface-emitting lasers (QC-VECSELs) have been recently demonstrated as a successful architecture to achieve scalable high output powers, high-quality beam patterns, and broad single-mode tuning.[10–13] The key component of a QC-VECSEL is an amplifying metasurface – a subwavelength reflectarray of metal-metal waveguide ridge antennas loaded with QC-gain material. The amplifying metasurface is further paired with an output coupler to form the external laser cavity, as sketched in Figure 1(a). Experiments have shown that QC-VECSELs "prefer" to lase in only one or two modes at a time.[14,15] The primary reason is that QC-VECSELs experience SHB in a fundamentally different way than waveguide-based QC-lasers.[14] The longitudinal modes primarily reside within the external cavity and each interacts with the gain material through the same metasurface resonance with nearly the same spatial overlap. This leads to effective gain clamping at lasing threshold, and typically only a single mode which is spectrally closest to the gain peak lases. As the cavity length is changed, two-mode operation is briefly seen as the main mode is detuned from the gain peak and a new mode begins to lase.[13] A secondary reason is that the partially transmitting output couplers used in intra-cryostat QC-VECSEL cavities often exhibit frequency-dependent reflectance characteristics; this adds to the differential gain needed for additional modes to reach lasing threshold. Third, diffraction loss has so far limited the maximum achievable intra-cryostat cavity lengths to a few millimeters such that the FSR $>$ 50 GHz; this exacerbates the previous two issues.

In this Letter, we demonstrate that multi-mode operation can be obtained in a QC-VECSEL by choosing a certain combination of output coupler and external cavity length in which the FSR of the cavity mode spectrum is nearly matched to a periodic reflectance spectrum of the output coupler. At certain cavity lengths, the frequency-dependent gain and reflectance at each external

cavity resonance frequency essentially compensate for each other, which allows for large sets of modes with nearly identical thresholds (although not necessarily compensated in dispersion). We experimentally observed up to nine lasing modes with an FSR as small as 21 GHz.

The underlying GaAs/$Al_{0.15}Ga_{0.85}As$ QC-active region was grown 10 μm thick by molecular beam epitaxy. It exhibits a broad gain characteristic peaking at 3.8 THz and is based upon the hybrid bound-to-continuum/resonant-phonon design scheme, first described in Ref. [16], and nominally identical to that in Ref. [15]. Microfabrication of the QC metasurface takes place in the standard metal-metal waveguide process, using a Cu-Cu thermocompression wafer bonding technique.[17] The metasurface design is a TM_{03} resonance design – first reported in Ref. [13] – where the width of each ridge antenna (32.5 μm) is approximately three half-wavelengths at resonance, and the ridge period is 65 μm. The metasurface was designed be resonant at 3.75 THz, which is close to the peak gain frequency of the QC-active material (see Supplementary Section S1). Modeling of the metasurface reflectance and reflection phase spectra was performed using full-wave 3D finite-element simulations (Ansys HFSS) and is plotted in Figure 1(b) supposing the metasurface is periodic and infinite and loaded with 30 cm^{-1} of frequency independent material gain. The size of the metasurface was deliberately made larger than previous demonstrations – 5×5 mm^2 in overall area where electrical bias is applied to a central circular area of 2.4 mm in diameter. The larger size reduces diffraction loss in a plano-plano cavity and allows longer length cavities (up to 12 mm in this case), although this comes at the cost of a large power dissipation. All measurements were performed at 77 K in pulsed mode with 0.5% duty cycle (1 μs pulses at 5 kHz repetition rate).

The first experiment was a "control," where a plano-plano VECSEL cavity was constructed using a planar mesh output coupler (OC) of the type that has been used in previous QC-VECSEL experiments.[18] The OC comprises an inductive Ti/Au mesh (10 μm period and 4 μm wide lines) evaporated on a 100-μm-thick double-side-polished quartz substrate, as sketched in Figure 1(c). While the mesh determines the overall transmittance magnitude, Fabry-Perot resonances within the quartz substrate lead to a slow modulation in transmittance (see Figure 1(d)); at 3.75 THz transmittance of 2% is measured. The output coupler was mounted inside the cryostat on a single-axis piezoelectric stepping stage (Attocube ANPx311) that can be used to adjust the cavity

length. The light and voltage vs. current (*L-I-V*) curves are plotted in Figure 1(e), where the power was collected with a pyroelectric detector (Gentec), and the absolute power levels were measured using a calibrated thermopile. The threshold current density is $J_{th} = 448$ A/cm^2, and the linear slope efficiency (dP/dI) is 192 mW/A (calculated by considering the 67% transmittance through the 3-mm-thick polyethylene cryostat window). The observed dynamic range was limited by the current limit (14 A) of the pulse generator, as a result larger powers could in principle be obtained. The lasing spectra were measured using a Fourier-transform infrared (FTIR) spectrometer with a resolution of 0.25 cm^{-1} shown in Figure 1(f). By stepping the piezoelectric stage, lasing spectra was tuned between 3.71 THz and 3.76 THz with an FSR of 21 GHz, which indicates a cavity length of $L_c \approx 7$ mm. Despite such a long cavity length, only two or three lasing

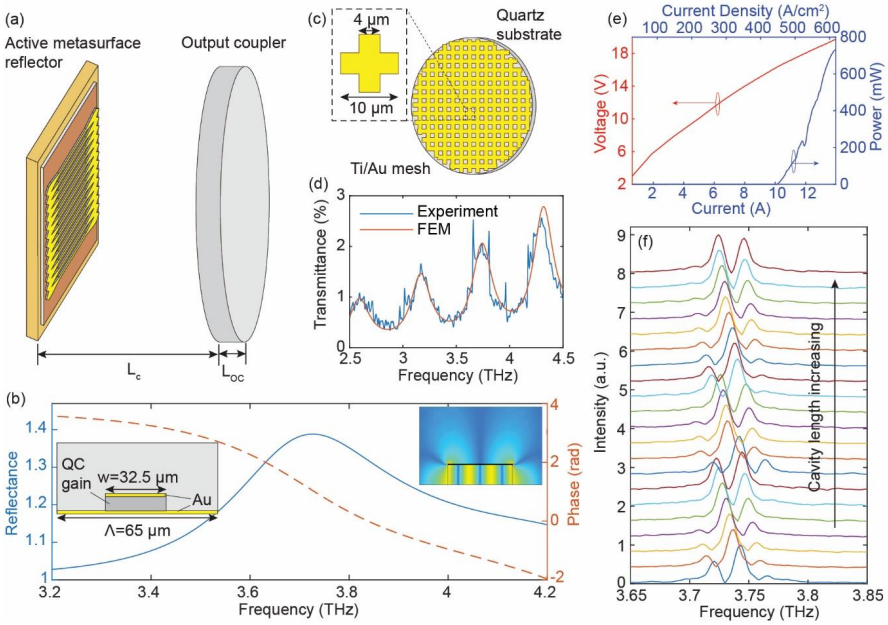

Figure 1. (a) Sketch of QC-VECSEL cavity consisting of the active QC-metasurface and the quartz output coupler. (b) FEM simulated reflectance (blue) and reflection phase (red dashed) spectra of amplifying TM_{03} metasurface with a ridge width of 32.5 μm and period of 65 μm, where 30 cm^{-1} of material gain is applied. (c) Sketch of inductive mesh quartz output coupler ($L_{OC} = 100$ μm) and (d) its experimental transmittance spectrum (blue) and analytical fitting (red). (e) Pulsed-mode *L-I-V* characteristics. (f) Normalized FTIR spectra at different cavity lengths, tuned by an intracryostat piezoelectric stage (offset for clarity). The device was biased at 12.6 A at 77 K.

modes were observed, spanning at most ~50 GHz – much narrower than the bandwidth of the metasurface (FWHM ≈ 300 GHz) and underlying gain material (~1 THz). Due to the lack of SHB, the QC-gain clamps at the lowest threshold gain coefficient and only modes experiencing the lowest lasing threshold will lase.

In order to promote multi-mode lasing, we replaced the thin quartz mesh output coupler with a mesh output coupler on a thick high-resistivity silicon substrate ($L_{oc} = 2.07$ mm), and adjusted the external cavity length to the condition $L_c \approx n_r L_{oc}$, in which the refractive index of silicon is taken as $n_r = 3.418$.[19] At this point the longitudinal modes of the cavity are approximately spectrally aligned with the reflectance peaks of the output coupler. To analyze how lasing modes develop as the relative position of the thick output coupler was tuned, we developed a simple multi-section cavity model which self-consistently calculates the cavity mode frequencies ν_m and their various threshold gains $g_{th,m}$ as L_c is varied, based upon the complex reflection coefficient of both the metasurface and output coupler (detailed description in Supplementary Section S2). To incorporate the effects of gain clamping phenomenologically, we assume that at least one mode with the lowest lasing threshold $g_{th,min}$ always lases, at which point the QC-gain clamps at $g_{cutoff} = g_{th,min} + \delta g$; a higher offset value δg indicates a lower degree of gain clamping.

The simulated lasing spectra are plotted in Figure 2(a) with respect to various cavity lengths from 6.4 to 7.4 mm. While the metasurface provides frequency-dependent amplification, lasing modes are determined by a Vernier selection mechanism between two coupled FP cavities – the external laser cavity and thick output coupler – each of which generates a series of longitudinal modes. More specifically, the standing waves within the output coupler substrate produce a periodic oscillation of effective reflectance spectrum R_{OC} which affects the threshold gain of the various cavity modes. If the two sets of modes have widely different frequency spacings (Case 1 shown in Figure 2(a)), only one cavity mode at a time sees the high effective reflectance from the output coupler, and mostly single mode behavior is predicted. As the cavity length is varied, lasing spectra are predicted to exhibit a combination of continuous frequency tuning punctuated by mode-hopping over one FSR and as well as a larger-scale mode-hopping over the metasurface bandwidth (between 3.65 THz and 3.9 THz). If the two sets of modes have nearly the same

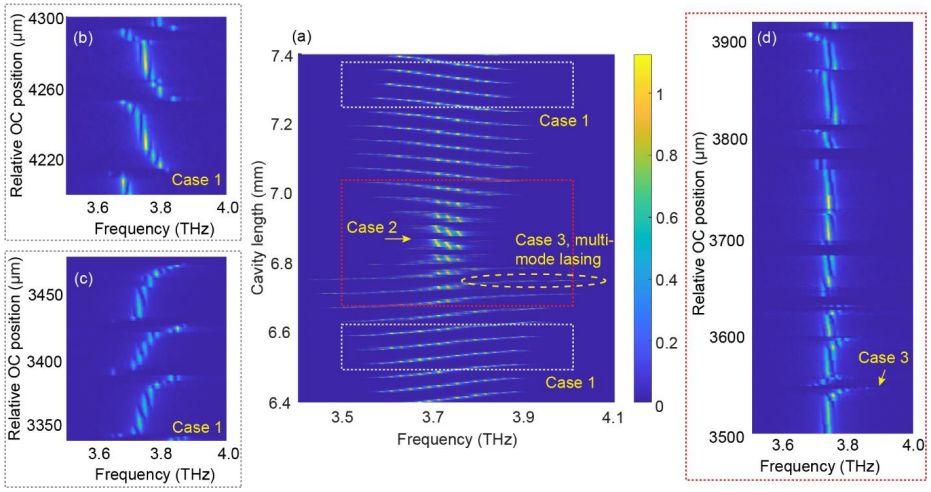

Figure 2. (a) Simulated lasing spectra of QC-VECSEL using the 2.07 mm thick silicon output coupler (Fig. 3 (a)) at different cavity lengths. δg is assumed as 0.15 cm^{-1}. Three cases are highlighted and are discussed in the text. Grey dotted boxes represent lasing spectra in Case 1, with corresponding experimental data plotted in (b-c) (biased at $I = 12.6$ A). Red dotted box represents lasing spectra in Case 3, with high likelihood of multi-mode lasing highlighted with yellow dashed circle. The experimentally demonstrated is plotted in (d).

frequency spacing (Case 2), multiple longitudinal cavity modes see similar effective output coupler reflectance, the lasing thresholds are now determined by the frequency-dependent metasurface reflectance and those modes closest to the gain peak will lase. It should be noted that perfect matching across the entire bandwidth is impossible, as the phase dispersion of the metasurface reflection reduces the cavity FSR near the metasurface resonance. However, there exists certain positions (Case 3) where the cavity lengths are slightly smaller than Case 2, and the combination of FP oscillation alignment and metasurface reflectance leads to a large number of modes with similar lasing thresholds. These are visualized as the multi-mode lasing "tails" as shown in the Figure 2(a) (yellow circle). One thing should be pointed out is that dispersion compensation is negligible as the phase difference between adjacent modes provided by the output coupler is too small compared to that of the metasurface (see Supplementary section S3).

The equivalent experiment was performed using TM_{03} metasurface paired with the output coupler shown in Figure 3(a). Various lasing spectra at different output coupler positions, i.e.

cavity lengths, are plotted in dotted boxes in Figure 2(b-d). Good qualitative agreement is observed with the simulated prediction, which confirms the Vernier tuning characteristics. Particularly, the lasing spectra around multi-mode lasing "tails" (pointed out by yellow arrow in Figure 2(d)) are emphasized and plotted in Figure 3(b-c). The red arrow in Figure 3(b) points out the output coupler position where the system suddenly shifts from two-mode lasing to multi-mode lasing with dense lasing modes covering over 170 GHz range. This phenomenon is sensitive to the external cavity length and disappeared as L_c was changed by only a few microns. It is also repeatable as the cavity length was tuned by approximately half-wavelength distances, where

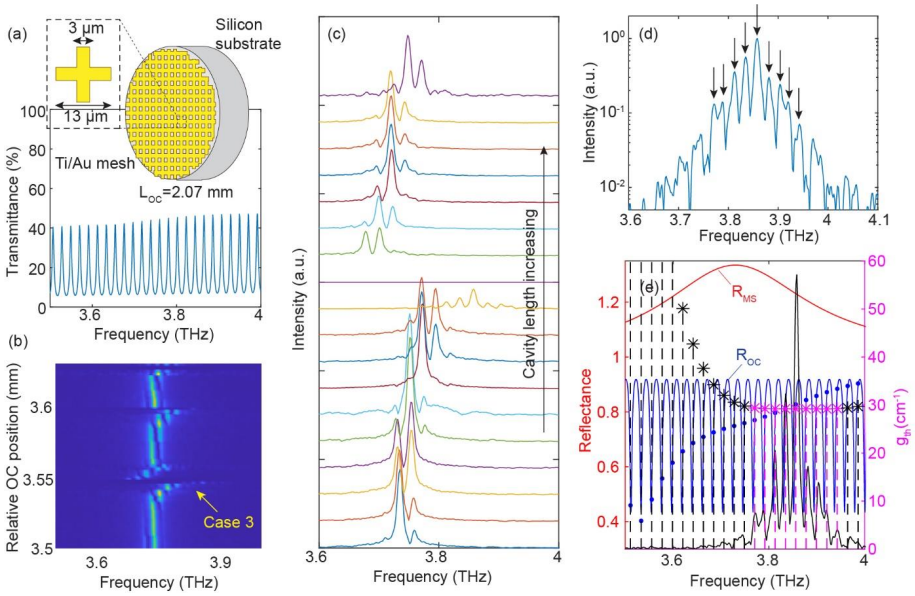

Figure 3. (a) FEM simulated transmittance of the silicon output coupler with a thickness of 2.07 mm. Inset shows the inductive mesh designed with a period of 13 μm and width of 3 μm. (b-c) Color plot and normalized lasing spectra (offset for clarity) measured at different cavity lengths. The device was biased at 12.6 A. The yellow arrow in (b) points out the cavity length where a sudden emergence of multiple lasing modes was observed. Log scale (d) and normalized (e) lasing spectra with up to nine lasing modes. In (e), black and magenta asterisks point out the theoretical lasing thresholds of longitudinal modes supported in the QC-VECSEL while we assume $L_c = 6.776$ mm to match the longitudinal resonances (magenta dashed lines) with the experimental lasing spectrum (black solid line). Magenta lines and asterisks are those lasing modes with thresholds $g_{th} < g_{cutoff}$, while black lines and asterisks represent those modes with $g_{th} > g_{cutoff}$ which could not lase. Blue and red curves represent the analytical reflectance of the output coupler and the TM_{03} metasurface at the lowest lasing threshold.

the lasing modes hopped back to their previous frequencies. One thing should be pointed out is that even though the piezoelectric stepper stage was operated in closed-loop condition, its resistive position sensor had limited resolution (estimated as approximately 1 μm) which led to some uncertainty in the absolute position and a few discontinuous jumps in the measured spectra.

The lasing spectrum with the most lasing modes is plotted in Figure 3(d) in log scale. We can distinguish at least nine lasing modes ranging from 3.77 THz to 3.94 THz, with an FSR around 21 GHz – this is the largest number of lasing modes ever observed in a QC-VECSEL. The frequency spacing between adjacent modes do not appear to be not exactly equidistant due to extra frequency-dependent phase shift provided by the QC-metasurface while the exact values are not measurable due to the limited resolution of the FTIR (see Supplementary section S3). The analytical lasing thresholds for each longitudinal mode in this multi-moding situation are plotted along with the experimental spectrum in Figure 3(e) (magenta asterisks) based on the multi-section cavity model (Supplementary Section S2), where the cavity length is assumed to be 6.776 mm in order to match the analytical longitudinal resonances with the experimental lasing peaks. At this specific cavity length, the output coupler reflectance seen by each longitudinal mode (blue dots) compensates for the frequency-dependent active reflectance of the QC-metasurface (red curve), which enables multiple modes with similar lasing threshold to lase simultaneously as experimentally demonstrated. The output power is also observed to drop slightly at this condition due to the increased threshold gain values at this condition.

This multi-moding phenomenon is repeatable using different output couplers both of different thicknesses (data for $L_{oc} = 1$ mm and 3 mm is presented in Supplementary Section S4) and of different reflectance. For example, in Figure 4 we consider a 2.07-mm-thick Si output coupler with a much more reflective mesh (period of 10 μm and width of 4 μm, see Figure 4(a)), which reduces the differential in threshold gains between the modes, and leads to a larger intracavity circulating intensity – estimated to be a few hundred W/cm^2. Figure 4(b) and 4(c) plot the lasing spectra at varying applied bias currents – ranging from a value slightly above lasing threshold ($I_{th} = 10.6$ A) to almost the maximum bias provided by the 14 A pulse generator (13.7 A), and the corresponding *L-I-V* curves. At lower biases, the amplification factor provided by the QC-

metasurface is smaller and can only support lasing mode around metasurface resonance resulting in single-mode operation. As the applied bias increases, more lasing modes were observed and the multi-mode regime appears to split into two in the spectra – a phenomenon similar to the Risken-Nummedal-Graham-Haken (RNGH) instability that has been observed in mid-IR QC-lasers.[9] Further study is needed to fully understand this phenomenon and its relationship to unique manifestation of SHB in the metasurface VECSEL. It is notable that no such phenomenon was observed when the more transmissive output coupler was used (Figure 3) – perhaps because of the lower intracavity circulating intensity.

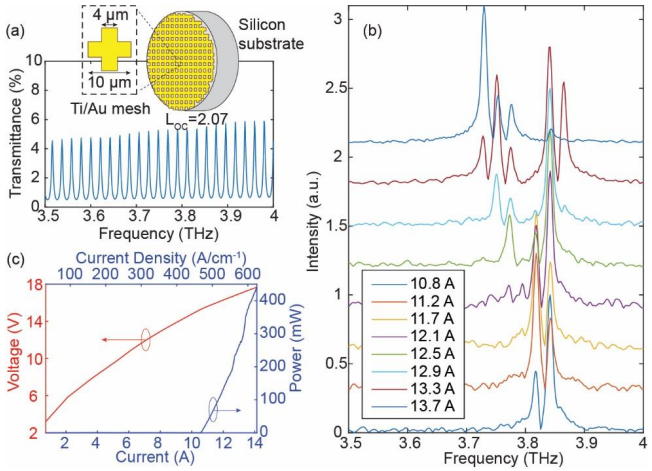

Figure 4. (a) Analytical transmittance of the silicon output coupler with a thickness of 2.07 mm. Inset shows the inductive mesh designed with a period of 10 μm and width of 4 μm. (b) Normalized lasing spectra at the cavity length supporting multiple lasing modes measured under different biases (offset for clarity). (c) Corresponding pulsed *L-I-V* curves measured at 77 K.

In this Letter, we have demonstrated a useful approach to promote multi-mode operation in QC-VECSELs by engineering the lasing thresholds for each longitudinal mode to be similar allowed by a certain combination of output coupler thickness and external cavity length. The dense multi-moding is a promising first step for eventual mode-locking/frequency-comb operation, as the FSR is in the range readily accessible for RF beatnote measurement and RF injection locking using modest instrumentations.[2,20] However, advances will be needed to reduce the metasurface power dissipation by 10x or more so that continuous-wave operation is possible. For example,

using a TM_{01} rather than a TM_{03} antenna metasurface will immediately reduce the power dissipation by 3×.[13] Also, the use of a patch-antenna (instead of ridge-antenna) based metasurface has been shown to reduce the power dissipation density by 2-4×.[21] Finally, by reducing the size of the metasurface biased area by 4× or more, the consumed power will be likewise reduced – although we anticipate that incorporating an intracavity mirror will be required to reduce diffraction for a smaller metasurface while maintaining a sufficiently long cavity length needed to ensure FSR < 25 GHz. On a separate note, future research should also investigate whether a higher degree of multi-moding can be achieved within QC-VECSELs by replacing this relative narrowband TM_{03} metasurface with either a broader-band and less dispersive single-element metasurface as in Ref. [12], or even an ultrabroadband coupled-resonator metasurface as in Ref. [15], which has exhibited a gain bandwidth over 1 THz and reduced group delay dispersion. Moreover, the engineered inhomogeneity present in the coupled-resonator metasurface may exhibit an increased degree of spatial hole burning in that different portions of the spectral profile are localized in different portions of the metasurface and is therefore favorable for multi-mode operation in QC-VECSELs.

Supplementary Material

See supplementary material for data on active region, detailed multi-section cavity model, discussion on dispersion, additional data collected using different output couplers and discussion on diffraction loss.

Acknowledgements

We thank Christopher Curwen for critical reading of the manuscript. Microfabrication was performed at the UCLA Nanoelectronics Research Facility and wire bonding was performed at the UCLA Center for High Frequency Electronics. This work was performed, in part, at the Center for Integrated Nanotechnologies, an Office of Science User Facility operated for the U.S. Department of Energy (DOE) Office of Science. Sandia National Laboratories is a multimission laboratory managed and operated by National Technology and Engineering Solution of Sandia, LLC., a wholly owned subsidiary of Honeywell International, Inc., for the U.S. Department of

Energy's National Nuclear Security Administration under contract DE-NA-0003525. Partial funding was provided by the National Science Foundation (1711892, 1810163, 2041165).

Data Availability

The data that supports the findings of this study are available within the article [and its supplementary material].

References:

[1] D. Burghoff, T. Y. Kao, N. Han, C. W. I. Chan, X. Cai, Y. Yang, D.J. Hayton, J. R. Gao, J. L. Reno, and Q. Hu, Nat. Photonics **8**, 462 (2014).

[2] S. Barbieri, M. Ravaro, P. Gellie, G. Santarelli, C. Manquest, C. Sirtori, S. P. Khanna, E. H. Linfield, and A. G. Davies, Nat. Photonics **5**, 306 (2011).

[3] J. Maysonnave, K. Maussang, J. R. Freeman, N. Jukam, J. Madéo, P. Cavalié, R. Rungsawang, S. P. Khanna, E. H. Linfield, A. G. Davies, H. E. Beere, D. A. Ritchie, S. S. Dhillon, and J. Tignon, Opt. Express **20**, 20855 (2012).

[4] A. Forrer, M. Franckié, D. Stark, T. Olariu, M. Beck, J. Faist, and G. Scalari, ACS Photonics **7**, 784 (2020).

[5] F. Wang, H. Nong, T. Fobbe, V. Pistore, S. Houver, S. Markmann, N. Jukam, M. Amanti, C. Sirtori, S. Moumdji, R. Colombelli, L. Li, E. Linfield, G. Davies, J. Mangeney, J. Tignon, and S. Dhillon, Laser Photonics Rev. **11**, 1 (2017).

[6] M. Rösch, G. Scalari, M. Beck, and J. Faist, Nat. Photonics **9**, 42 (2014).

[7] C. L. O'Bryan and M. Sargent, Phys. Rev. A **8**, 3071 (1973).

[8] H. A. Haus, IEEE J. Sel. Top. Quantum Electron. **6**, 1173 (2000).

[9] A. Gordon, C. Y. Wang, L. Diehl, F. X. Kärtner, A. Belyanin, D. Bour, S. Corzine, G. Höfler, H. C. Liu, H. Schneider, T. Maier, M. Troccoli, J. Faist, and F. Capasso, Phys. Rev. A - At. Mol. Opt. Phys. **77**, 1 (2008).

[10] L. Xu, C. A. Curwen, P. W. C. Hon, Q. -S. Chen, T. Itoh, and B. S. Williams, Appl. Phys. Lett. **107**, 221105 (2015).

[11] L. Xu, D. Chen, T. Itoh, J. L. Reno, and B. S. Williams, Opt. Express **24**, 24117 (2016).

[12] C. A. Curwen, J. L. Reno, and B. S. Williams, Nat. Photonics **13**, 855 (2019).

[13] C. A. Curwen, J. L. Reno, and B. S. Williams, Appl. Phys. Lett. **113**, 011104 (2018).

[14] L. Xu, C. A. Curwen, D. Chen, J. L. Reno, T. Itoh, and B. S. Williams, IEEE J. Sel. Top. Quantum Electron. **23**, 1200512 (2017).

[15] C. A. Curwen, J. L. Reno, and B. S. Williams, Electron. Lett. **56**, 1264 (2020).

[16] M. I. Amanti, G. Scalari, R. Terazzi, M. Fischer, M. Beck, J. Faist, A. Rudra, P. Gallo, and E. Kapon, New J. Phys. **11**, 125022 (2009).

[17] B. S. Williams, S. Kumar, Q. Hu, and J. L. Reno, Opt. Express **13**, 3331 (2005).

[18] L. Xu, C. A. Curwen, J. L. Reno, and B. S. Williams, Appl. Phys. Lett. **111**, 101101 (2017).

[19] J. Dai, J. Zhang, W. Zhang, and D. Grischkowsky, J. Opt. Soc. Am. B **21**, 1379 (2004).

[20] A. Mottaghizadeh, D. Gacemi, P. Laffaille, H. Li, M. Amanti, C. Sirtori, G. Santarelli, W. Hänsel, R. Holzwart, L. H. Li, E. H. Linfield, and S. Barbieri, Optica **4**, 168 (2017).

[21] C. A. Curwen, J. L. Reno, and B. S. Williams, Appl. Phys. Lett. **116**, 241103 (2020).